MULTI-FREQUENCY LINBO$_3$ LAMB WAVE RESONATORS WITH < 3Ω IMPEDANCE

Renyuan Wang[1], Sunil A. Bhave[2], Sergei Zhgoon[3] and Kushal Bhattacharjee[4]
[1]Cornell University, Ithaca, NY, USA
[2]Purdue University, West Lafayette, IN, USA
[3]Moscow Power Engineering Institute, Moscow, Russia
[4]Qorvo Inc., Greensboro, USA

ABSTRACT

This paper presents monolithic multi-frequency $LiNbO_3$ (LN) Lamb wave resonators fabricated on a 3in. X-cut thin-film LN-SiO2-LN wafer. Resonators with four different frequencies (667MHz, 793MHz, 846MHz, and 713MHz) are demonstrated. While resonators with the first three frequencies operate in 0th order symmetric (S_0) Lamb wave mode, resonators with the last frequency utilize the 0th order shear horizontal (SH_0) Lamb wave. Exploiting a long transducer design, the resonators exhibits spur-suppressed response, <3Ω impedance at resonance, and electromechanical coupling factor (k_{eff}^2) >17% without any de-embedding, and the highest k_{eff}^2 achieved is 24.1%.

INTRODUCTION

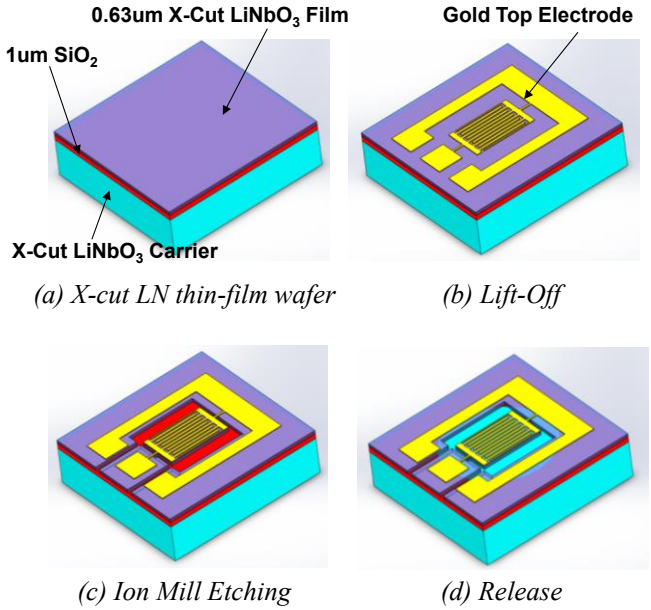

(a) X-cut LN thin-film wafer *(b) Lift-Off*

(c) Ion Mill Etching *(d) Release*

Figure 1: Fabrication Process of the Lamb wave resonator: (a) Starting with 3in. X-cut LN-SiO$_2$-LN wafer; (b) Define top electrodes by lift-off; (c) Define device geometry by ion milling; (d) Release the devices in BOE and dry in critical point dryer (CPD).

Filters made from bulk acoustic wave resonators have become the dominant technology for high-band filtering solutions in mobile wireless communication devices. As the number of supported bands increases in a single mobile device, it has become increasingly complex to achieve a single packaged RF frond-end solution using BAW technology. This is due to the fact that the frequency of BAW filters is determined by the thickness of the epitaxially deposited piezo, metal and dielectric layers that constitutes the resonators which makes monolithic integration of devices with multiple frequencies challenging. Therefore, the popular approach to achieve a single packaged solution supporting multiple bands is to pick and mount filter chips for different bands on a common laminate.

To achieve monolithic integrated multi-frequency band-pass filters, Lamb wave resonators have been proposed. To achieve competitive filtering performance against BAW filters, the resonators need to exhibit spur-suppressed response, high $k_{eff}^2 \times Q$, and resonant impedances as close to zero as possible. Previous works [1-4] have shown that Lithium Niobate Lamb wave devices have great potential in satisfying all above requirements. However, to date, none of the devices fabricated by surface micro-machining have shown less than 20Ω impedance at resonance and greater than 12% k_{eff}^2 without de-embedding the pad capacitance. In addition, LN thin-films generally can support multiple acoustic mode types and Lamb wave resonators generally operate at high-order harmonic modes of the resonator body. Therefore, managing spurious modes is more challenging for such devices. To further advance the performance of LN Lamb wave resonators, we use optimized long transducer designs on a 3 in. x-cut $LiNbO_3$ thin-film wafer to achieve LN Lamb wave resonators with spur-suppressed response and low resonant impedance. Taking advantage of LN's strong piezoelectric coupling of S_0 and SH_0 modes, the resonators also exhibits high k_{eff}^2 without any de-embedding.

FABRICATION

We start the fabrication with a 3in. X-cut LN piezo-on-insulator (POI) wafer (Fig. 1a), which has a 0.63um thick X-cut LN thin-film on top of X-cut LN substrate with a 1um thick PECVD SiO_2 sacrificial layer. The LN thin-film is fabricated using the ion-slice technique, where the ion-implanted device wafer deposited with PECVD oxide is directly flip-bonded on the carrier and heat treatment is used to separate the thin-film from the device wafer. Fig. 2a shows the starting thin-film wafer, which shows no interference pattern indicating very good film thickness uniformity. Next, we define the gold top electrode by lift-off. A thin sputtered chromium layer was used to improve the adhesion of gold. Then, we use ion mill etching to define the device geometry with photoresist mask [2]. The ion mill utilizes an 8 in. uniform beam ICP Argon ion source, which ensures the whole wafer is etched uniformly. In addition, the wafer is mounted on water cooled chuck to prevent sample over-

heating. Finally, the devices are released in BOE 6:1 and critical point dryer. The inset in Fig. 2b shows a photo of the wafer after ion mill etching, and Fig. 2c shows the fully released device. Multiple tethers were used to properly suspend the device preventing it from attaching to the substrate. Except for the resonator boundary at the very end of the transducer, all corners of the device geometry are rounded to help prevent creation of stress-induced cracks from sharp corners in the geometry. As shown in Fig. 2d, the ion mill produced smooth etching profile which mitigates acoustic scattering loss at the boundaries.

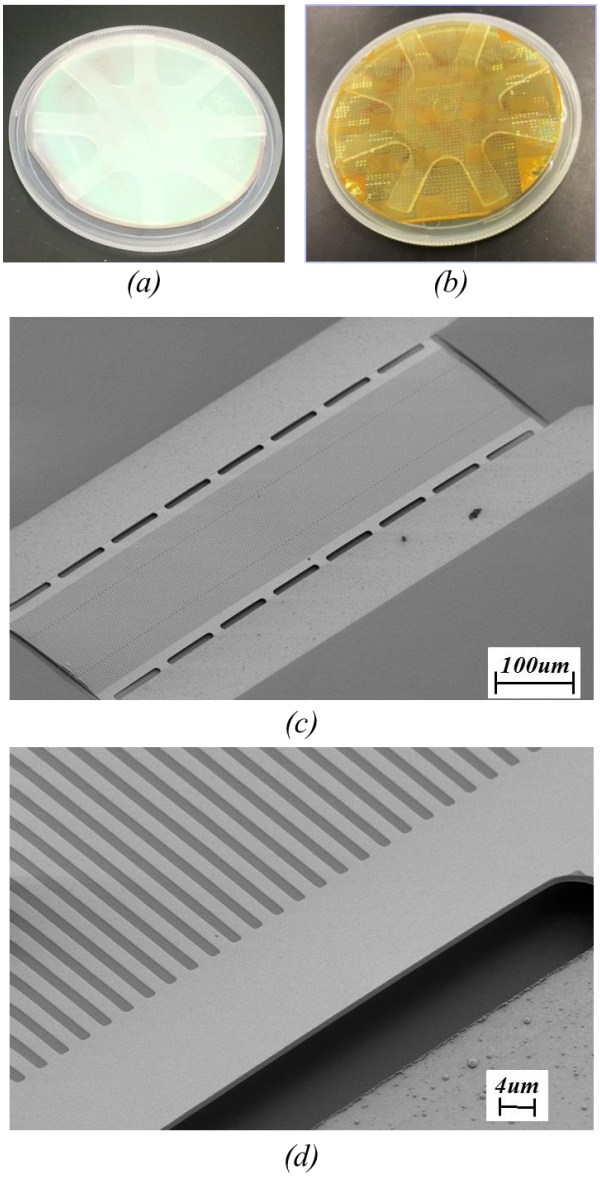

Figure 2: Photos of the wafer during different stages of fabrication and SEMs of the released resonator.

DESIGN

Depending on the orientation of the transducer, either S_0 [1] or SH_0 [3] modes can be efficiently excited on X-cut LN thin film. As the maximum electromechanical couplings for the two modes do not coincide at the same transducer orientation, it's possible to optimize the transducer to achieve maximum coupling for a particular mode. However, it's important to note that the coupling factor for the other mode generally doesn't go to zero at the same time which causes spurious response in the spectrum. Therefore, trade-off and careful design are required to achieve good coupling factor for the targeted mode while suppressing the spurious response. For example, Fig. 3 shows the admittance spectrum of the resonator at different transducer orientations from 3D finite element simulation. The resonators are targeted to operate in the S_0 mode. When the transducer fingers are aligned at 30° from z+ to y-, the resonator exhibits highest coupling factor of 31% calculated using the equation: $k_{eff}^2 = \pi/2 \cdot f_s/f_p \cot(\pi/2 \cdot f_s/f_p)$. However, the SH_0 mode is also excited with a k_{eff}^2 of 2% which causes an out-of-band spur. On the other hand, the coupling factor for SH_0 mode diminishes when the fingers are aligned at 40° from z+ to y-, and the k_{eff}^2 of S_0 mode is only reduced by 1% to 30%. As a result, the majority of the S_0 mode resonators are designed to have IDTs oriented along 40° from z+ to y-. The optimization effort was mainly toward achieving good k_{eff}^2 while minimizing spurs caused by modes other than the targeted acoustic mode. Such spurs generally appear far away in the spectrum from the targeted resonance due to large difference in the acoustic velocities. For example, the S_0 wave travels approximately 1.58 times faster than SH_0 mode in our design. However, we did not aim to minimize spurs caused by the transverse modes (same acoustic mode type as the targeted mode but with wave vectors non-perpendicular to the IDTs) which manifest themselves as in-band spurs. There is yet another type of spurs, which are caused by the same mode type of the targeted one but with different harmonic orders, which will be discussed in the last paragraph of this section.

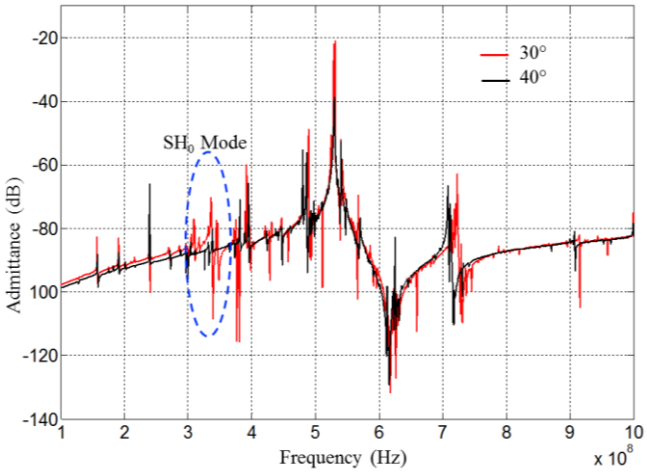

Figure 3: Resonator admittance spectrum as a function of IDT orientation from 3D finite element simulation.

For the SH_0 resonator, we performed similar analysis. The SH_0 mode exhibits the highest k_{eff}^2 (32%) when IDTs are oriented at 10° from z+ to y+. However, the A_0 and S_0 modes are also excited at this angle with less than 3% of k_{eff}^2, and it's very hard to suppress both modes without significantly affecting the k_{eff}^2 of the SH_0 mode. Therefore, the SH_0 mode resonators are designed to

achieve highest k_{eff}^2. One note of caution is that the piezoelectric coupling of x-cut LN does not have mirror symmetry with respect to either y axis or z axis. However, the wafer major flat is generally perpendicular to the z axis. Therefore, it's important to pay special attention to the wafer rotation angle during photolithography.

Finally, it's crucial to achieve a resonant impedance as close to zero as possible to minimize filter insertion loss. Increasing the number of the fingers (or the length) of the interdigital transducer leads to larger device area resulting in lower resonant impedance and increased device capacitance which minimizes the impact of pad capacitance on k_{eff}^2. However, simply increasing transducer length may lead to more spurious resonator response due to transversely confined modes and the competition between the two sets of boundary conditions: one from mechanical scattering of the transducer fingers, and one from the etched reflective boundaries of the resonators [5]. Here, we implement optimized long transducer designs to achieve resonators with low resonant impedance, high k_{eff}^2, and spur-suppressed responses at the same time. Intuitively, the anisotropically etched device boundaries give frequency independent reflective boundary conditions while the acoustic scattering from IDT fingers is periodic, thus frequency selective. In the meantime, IDTs are frequency selective transducers. The bandwidths of the IDT transduction window and reflection window generally go inversely with increasing total number of fingers, and a properly designed long IDT can provide highly frequency selective transduction and reflection, thus resulting in strong suppression of harmonic modes of the target mode and spur-suppressed response.

EXPERIMENT RESULTS

Fig. 2c shows the fully released S_0 mode resonator with IDTs oriented at 40° from z+ to y-. The resonators are measured using a network analyzer. Fig. 4 shows the measured admittance spectrum of three resonators fabricated on the x-cut thin film wafer designed for three different frequencies (667MHz, 793MHz, and 846MHz), and table 1 summarizes their performance. Their corresponding acoustic wavelengths are 3.6um, 3um and 2.8um, respectively. Using the same equation, we calculate their corresponding coupling factor to be 19.6%, 17.8% and 19.4% respectively. As we do not perform any de-embedding, the coupling factors are consistent with our simulation when taking into account of the pad capacitance. The length direction of the IDT fingers is marked by the blue arrow, which is at 40° from z+ to y-. As predicted by our analysis, all three resonators exhibit clean spectrum. However, they do exhibit in-band spurs caused by transversely confined modes. Because of the long transducer design, all devices exhibit less than 3Ω of impedance at resonance (2.17Ω for 667MHz, 2.65Ω for 793MHz and 2.45Ω for 846MHz).

In addition, we also compare the response of resonators with different IDT orientations (30° and 40° from z+ to y-) as shown in Fig. 5. As expected from our modeling, the spectrum of resonator A (IDT at 30° from z+ to y-) exhibits a strong spur at 432MHz caused by the SH_0 mode while the targeted S_0 resonance is at 665MHz.

Table 1: Summary of S_0 mode resonator performance.

	f_s (MHz)	f_p (MHz)	R_s (Ω)	k_{eff}^2 (%)	Q
—	667	730	2.17	19.6	210
—	793	860	2.65	17.8	170
—	846	925	2.45	19.4	160

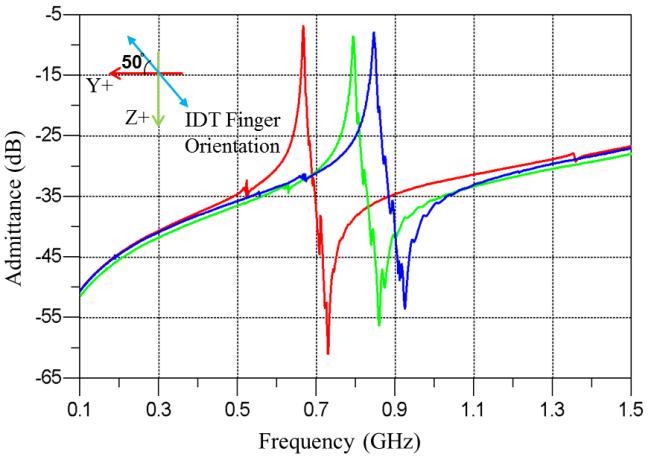

Figure 4: Measured admittance spectrum of resonators at different frequencies.

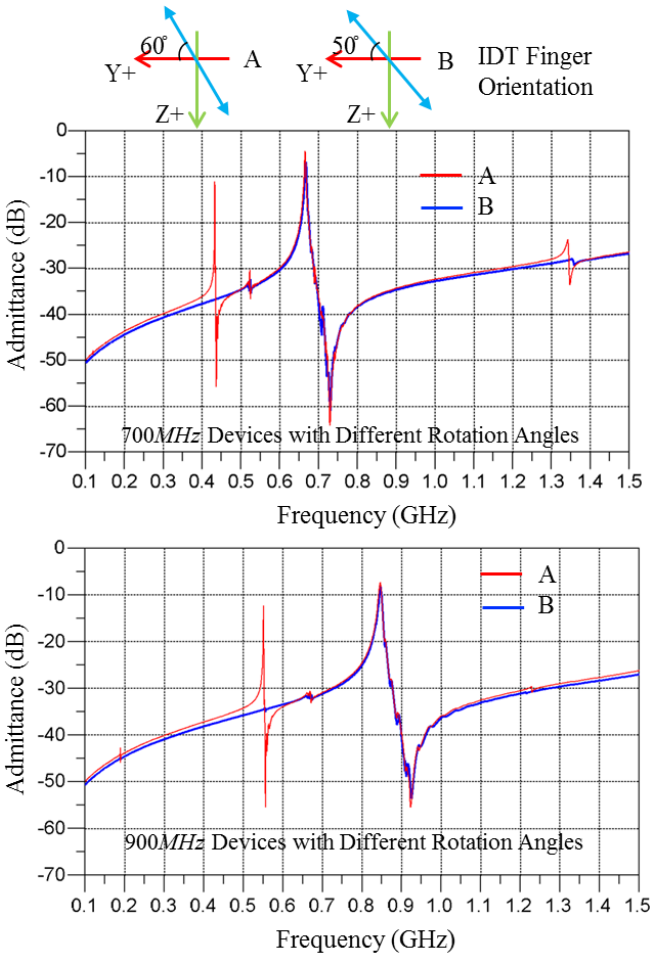

Figure 5: Measured admittance spectrum of S_0 resonators with different resonant frequencies and rotation angles.

In contrast, the SH_0 mode for device B with IDT at 40° from z+ to y- is strongly suppressed. Similarly for devices with acoustic wavelength of 2.8um, the resonator

with IDT oriented at 30° from z+ to y- has a strong SH_0 spur at 551MHz and the S_0 resonance is at 846MHz while the optimized IDT design only shows one strong resonance from S_0 mode at 846MHz.

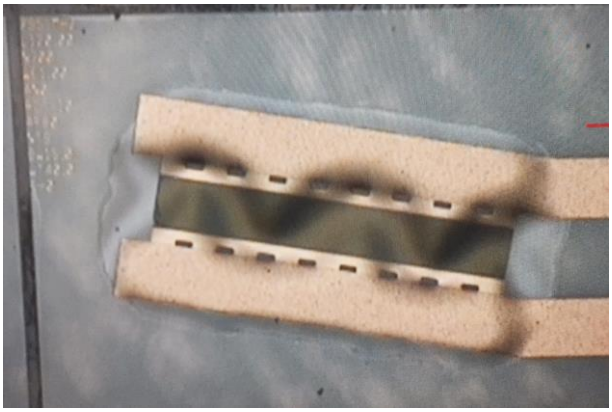

Figure 6: Microscopic photo of a fully released SH_0 mode resonator.

Finally, Fig. 6 shows the fully released SH_0 mode resonator with the IDTs oriented at 10° from z+ to y+, while Fig. 7 shows the measured admittance spectrum. The main resonance from the SH_0 mode is at 713MHz with a corresponding acoustic wavelength of 2.2um which is a result of the much slower acoustic velocity of SH_0 mode as compared to S_0 mode. This makes photolithography more challenging for these devices. The coupling factor calculated using the same formula is 24.1% without any de-embedding, and the impedance at resonance is 1.71Ω with a Q of 125. However, as expected from our modeling, the spectrum exhibits two strong spurs at 353MHz and 1189MHz which are caused by the parasitic excitation of A_0 and the S_0 modes.

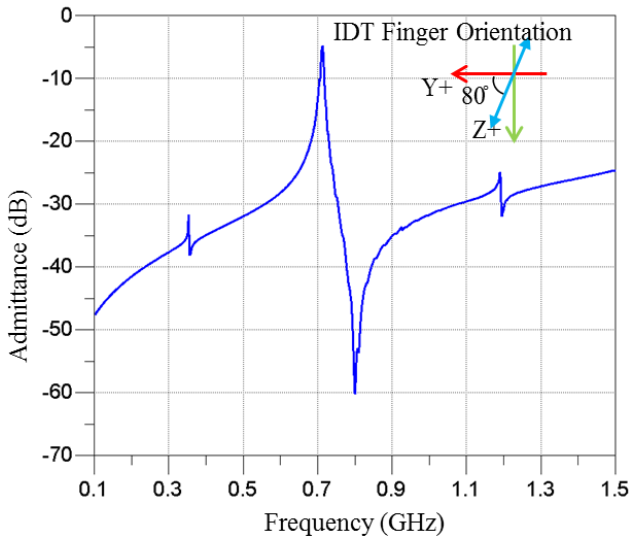

Figure 7: Measured admittance spectrum of the SH_0 mode resonator.

CONCLUSION

In this work, we demonstrate LN Lamb wave resonators on an x-cut thin-film $LiNbO_3$ wafer with different resonant frequencies and operating in different acoustic modes. We use optimized long transducer designs to achieve spur-suppressed frequency response, less than 3Ω impedance at resonance, and over 17% k_{eff}^2 without any de-embedding, while the highest k_{eff}^2 achieved is 24.1%. By carefully controlling the etch and release parameters, designing stress relief suspensions, and choosing the appropriate X-cut LN orientation, we have demonstrated single-chip multi-frequency MEMS resonators with < 3 Ohm impedance.

ACKNOWLEDGEMENTS

This work was performed in part at the Cornell NanoScale Facility, a member of the National Nanotechnology Coordinated Infrastructure (NNCI), which is supported by the National Science Foundation (Grant ECCS-15420819).

REFERENCES

[1] S. Gong and G. Piazza, "Design and analysis of lithium-niobate based high electromechanical coupling RF-MEMS resonators for wideband filter", *MTT, IEEE Tran. on*, vol. 61, pp. 403-414, 2013.

[2] R. Wang, S. A. Bhave, and K. Bhattacharjee, "Design and fabrication of S_0 Lamb-wave thin-film lithium niobate micromechanical resonators", *J. Microelectromech. Syst.*, vol. 24, pp. 300-308, 2015.

[3] R. H. Olsson III, K. Hattar, S. J. Homeijer, M. Wiwi, M. Eichenfield, D. W. Branch, M. S. Baker, J. Nguyen, B. Clark, T. Bauer, T. A. Friedmann, "A high electromechanical coupling coefficient SH_0 Lamb wave lithium niobate micromechanical resonator and a method for fabrication", *Sensors and Actuators A: Physical*, vol. 209, pp. 183-190, 2014.

[4] M. Kadota, M. Esashi, S. Tanaka, Y. Kuratani, and T. Kimura, "High frequency resonators with wide bandwidth using SH_0 mode plate wave in thin $LiNbO_3$," in *Digest Tech. Papers Ultrasonics Symposium*, Prague, July 21-25, 2013, pp. 1680-1683.

[5] R. Wang, S. A. Bhave, and K. Bhattacharjee, "Modeling of interdigitated transducer for high-order contour-mode resonators," in *Digest Tech. Papers Ultrasonics Symposium*, Prague, July 21-25, 2013, pp. 1926-1929.

CONTACT

*R. Wang, tel: +1-607-793-0877;
renyuan.wang@qorvo.com